Proton interchange tunneling and internal rotation in HSH–NH3

G. Hilpert, G. T. Fraser, R. D. Suenram, and E. N. Karyakin

Citation: The Journal of Chemical Physics **102**, 4321 (1995); doi: 10.1063/1.469480
View online: http://dx.doi.org/10.1063/1.469480
View Table of Contents: http://scitation.aip.org/content/aip/journal/jcp/102/11?ver=pdfcov
Published by the AIP Publishing

Proton interchange tunneling and internal rotation in HSH–NH_3

G. Hilpert,[a] G. T. Fraser, and R. D. Suenram
Molecular Physics Division, National Institute of Standards and Technology, Gaithersburg, Maryland 20899

E. N. Karyakin
Molecular Spectroscopy Laboratory, Applied Physics Institute, Nizhnii Novgorod, Russia

(Received 10 November 1994; accepted 7 December 1994)

An electric-resonance optothermal spectrometer and phase-locked backward-wave oscillators are used to investigate the *b* type, $\Delta K=\pm 1$, $\Delta m=0$ spectrum of the hydrogen-bonded HSH--NH_3 and $H^{34}SH$--NH_3 complexes near 300 GHz. The spectrum is characterized by nearly free internal rotation of the NH_3 subunit against the H_2S, as initially concluded from Stark-effect measurements by Herbine *et al.* [J. Chem. Phys. **93**, 5485 (1990)]. Transitions are observed for the $K=1\leftarrow 0$, $m=0$, *A* symmetry and the $K=0\leftarrow\pm 1$ and $K=\pm 2\leftarrow\pm 1$, $m=\pm 1$, $Km>0$, *E*-symmetry subbands. The transitions are split into doublets with a 3:1 relative intensity ratio indicative of tunneling interchange of the two H_2S protons. The observed selection rules, symmetric $\leftrightarrow$ antisymmetric in the tunneling state, indicate that the tunneling motion reverses the sign of the molecular electric dipole moment component along the *b* inertial axis. The most likely interchange motion consists of a partial internal rotation of the H_2S unit about its *c* inertial axis, through a bifurcated, doubly hydrogen-bonded transition state. The proton interchange tunneling splittings of 859–864 MHz vary little between *K* and *m* states, indicating that the interchange motion is only weakly coupled to the internal rotation. The barrier to proton interchange is determined to be 510(3) cm^{-1}, which can be compared to the $\sim$700 cm^{-1} barrier estimated from the 57 MHz tunneling splittings associated with the H_2O proton interchange in the related HOH--NH_3 complex. The observation of dissociation of HSH--NH_3 following excitation of the NH_3 umbrella mode with a line-tunable CO_2 laser places an upper bound of 992 cm^{-1} on the hydrogen-bond zero-point dissociation energy. The band origin for the umbrella vibration of 992.5(10) cm^{-1} is blueshifted by 43 cm^{-1} from the hypothetical inversion-free band origin of uncomplexed NH_3. Previous studies have shown that the HOH--NH_3 binding energy is greater than 1021 cm^{-1}. © *1995 American Institute of Physics.*

INTRODUCTION

In the past two decades significant progress has been made toward a detailed description of the hydrogen bonding interactions of the first-row hydrides.[1] Microwave and infrared spectroscopy has been used to study the structure and dynamics of HF, H_2O, and NH_3 complexes, and the results have driven improvements in *ab initio* calculations and dynamical theories so that now quantitative comparisons between high-level theory and the extremely accurate experimental measurements are possible. Less attention has been given to the second row hydrides, particularly H_2S and PH_3, in part, due to their decreased chemical importance. However, because of their large number of electrons, both H_2S and PH_3 complexes offer an important challenge to *ab initio* theory to accurately model their structures and force fields.

In contrast to the first-row hydrides, where electrostatic forces dominate the binding, the second-row hydrides have large dispersion contributions to their interactions. The intermolecular force fields of the hydrogen bonding interactions of the second-row hydrides are thus expected to be less directional than their corresponding first-row partners. This is seen in the comparison of the dimers of HF[2] and HCl,[3] where the hydrogen-bond donor–acceptor interchange tunneling in $(HF)_2$ is more than an order of magnitude less than in $(HCl)_2$ due to the more anisotropic potential-energy surface of the $(HF)_2$.

In the case of H_2O complexes of the form HOH--B, where B is a Lewis base, one measure of the directionality of the hydrogen bonding is the tunneling splitting associated with the interchange of the two protons on the water subunit. This tunneling splitting has been directly measured by molecular-beam far-infrared spectroscopy for the complexes of H_2O with CO,[4] N_2,[5] and NH_3[6] and by microwave and submillimeter spectroscopy for $(H_2O)_2$.[7] Here, the tunneling splittings are found to range from 31 GHz for the N_2 complex to 57 MHz for the NH_3 complex.

For the corresponding H_2S complexes, little effort has been made to investigate the directionality of the HSH--B hydrogen bond. This information could be inferred from measurements of the *b*-type submillimeter rotation-tunneling spectrum of the dimer which allows the direct observation of the HSH proton interchange tunneling splitting. To investigate this tunneling motion in an H_2S complex, in the present study we examine the *b*-type rotation tunneling spectrum of the HSH--NH_3 complex using a molecular-beam electric-resonance spectrometer[8,9] with phase-locked backward-wave oscillator (BWO) submillimeter sources.[10] A previous microwave study by Herbine *et al.*[11] at frequencies below 20 GHz allowed the observation of the $\Delta K=0$ transitions of the complex, revealing a nearly linear N--H–S hydrogen-bonded structure with essentially free internal rotation of the H_3N subunit about its C_3 symmetry axis, similar to results ob-

[a]Permanent address: Institut für Angewandte Physik, Wegelerstr. 8, 53115 Bonn, Germany.

tained for the related HOH--NH_3 complex. No conclusive evidence was found for the H_2S proton interchange tunneling in the microwave study.

For HSH--NH_3, the $\Delta K=0$ rotational transitions observed by Herbine *et al.*[11] do not directly probe the HSH proton interchange tunneling since the *a* inertial axis component of the molecular electric dipole moment is a symmetric function of the tunneling coordinate. Because the *b* dipole moment component is an antisymmetric function of the tunneling coordinate, the *b* type, $\Delta K=\pm 1$, transitions, which are expected to lie in the submillimeter region near 300 GHz, allow a direct measure of this tunneling splitting.

In the present study, we find a tunneling splitting of ~860 MHz for the HSH proton interchange tunneling in HSH--NH_3. This splitting can be compared to the much smaller splitting of 57 MHz observed by Stockman *et al.*[6] for the HOH--NH_3 complex. For the H_2S complex the observed splitting implies a barrier of 510(3) cm^{-1}, which is significantly lower than the ~700 cm^{-1} barrier determined by Stockman *et al.*[6] These results are consistent with previous conceptions that the first row hydrides form much more directional hydrogen bonds than their corresponding second row partners. Finally, CO_2-laser molecular-beam depletion studies of the ammonia umbrella vibration of the complex place an upper bound of 992 cm^{-1} on the hydrogen-bond dissociation energy. For HOH--NH_3 previous infrared studies[12] place a lower bound of 1021 cm^{-1} on the HOH--NH_3 bond dissociation energy.

EXPERIMENT

The electric-resonance optothermal spectrometer used in the present investigation has been described previously.[8,9] Briefly, a molecular beam of HSH--NH_3 is formed by a room-temperature expansion of a mixture of 3% ammonia and 3% hydrogen sulfide in helium through a 40 μm pinhole nozzle, resulting in a rotational temperature of 5–10 K. The molecular beam is collimated by a 1 mm diameter skimmer and then focused or collected by a 56 cm long electrostatic lens of quadrupole symmetry onto a 1.7 K liquid-He-cooled bolometer detector[13] located approximately ~90 cm from the nozzle. Between the nozzle and skimmer, microwave or submillimeter radiation is applied to the molecular beam using a cutoff section of *K*-band waveguide. For double-resonance studies, radiofrequency radiation between 10 MHz and ~7 GHz can also be simultaneously applied via a wire antenna.

Microwave/radiofrequency radiation below 40 GHz is provided directly by a computer controlled 10 MHz–26.5 GHz frequency synthesizer or by doubling and amplifying the output of the synthesizer. Several milliwatts of radiation from 230 to 380 GHz is supplied by backward-wave oscillators phase locked to a harmonic of a 2–18 GHz frequency synthesizer.[10] The microwave/submillimeter radiation is either frequency or amplitude modulated for phase-sensitive detection of the bolometer output. The signal strength is a function of the usual Hönl–London and Boltzmann factors, as well as the focusing characteristics of the upper and lower states of the transitions in the quadrupole field.

CO_2-laser photodissociation spectra of HSH--NH_3 were measured using a line-tunable CO_2 laser. Spectra were obtained by multiply crossing the molecular beam between the nozzle and skimmer with a 6–8 W CO_2 laser beam. The photodissociation signal strength varies with the quadrupole-field voltage verifying that the carrier of the signal is a polar complex.

RESULTS AND DISCUSSION

The submillimeter spectrum of HSH--NH_3 is complicated by the nearly free internal rotation of the NH_3 top against the off-axis nonbonded HS bond and by the tunneling interchange of the protons of the H_2S subunit. These same types of tunneling and internal-rotation features are also seen in the spectroscopy of H_3N--H_2O.[12,14,15] Before discussing the present results it is useful to briefly review the spectroscopic theory of such a highly nonrigid complex.

Internal rotation theory

The rotation–internal-rotation Hamiltonian for a molecule with a plane of symmetry and a symmetric internal rotor can be written as[16,17]

$$H=A\mathbf{J_a^2}+B\mathbf{J_b^2}+C\mathbf{J_c^2}-2Q\mathbf{jJ_a}-2N_{\mathbf{j}}\mathbf{J_b}+G(\mathbf{J_aJ_b}+\mathbf{J_bJ_a}) +F\mathbf{j}^2+V(\alpha), \tag{1}$$

where $\mathbf{J}_a$, $\mathbf{J}_b$, and $\mathbf{J}_c$ are the projections of the total angular momentum, $\mathbf{J}$, onto the rigid-molecule principal inertial axes, $\mathbf{j}$ is the angular momentum of the NH_3 top along its symmetry axis, and α is the internal-rotation angle. The rotational and Coriolis constants are defined as,

$$A=\left(1+\frac{\lambda_a^2 I_\alpha}{rI_a}\right)\frac{\hbar^2}{2I_a},\quad B=\left(1+\frac{\lambda_b^2 I_\alpha}{rI_b}\right)\frac{\hbar^2}{2I_b},$$
$$C=\left(1+\frac{\lambda_c^2 I_\alpha}{rI_c}\right)\frac{\hbar^2}{2I_c},\quad F=\frac{\hbar^2}{2rI_\alpha},\quad N=\frac{\hbar^2\lambda_b}{2rI_b},$$
$$Q=\frac{\hbar^2\lambda_a}{2rI_a},\quad G=\frac{\hbar^2\lambda_a\lambda_b I_\alpha}{2rI_aI_b}, \tag{2}$$

where

$$r=1-\frac{\lambda_a^2 I_\alpha}{I_a}-\frac{\lambda_b^2 I_\alpha}{I_b}. \tag{3}$$

Here, I_a, I_b, and I_c are moments of inertia of the rigid complex about the *a*, *b*, and *c* principal axes, I_α is the moment of inertia of the NH_3 top about its symmetry axis, and λ_a and λ_b are the direction cosines between the top axis and the molecular *a* and *b* axes of the complex. The internal rotation potential is approximated as

$$V(\alpha)=\frac{V_3}{2}(1-\cos 3\alpha), \tag{4}$$

where V_3 is the barrier to internal rotation. Matrix elements of H are evaluated in the free-rotor basis set $|JKMm\rangle=|JKM\rangle e^{im\alpha}(2\pi)^{-1/2}$ where $|JKM\rangle$ is a prolate-top symmetric rotor function and m is an eigenvalue of $\mathbf{j}$. The Hamiltonian matrix factors into A and E symmetry

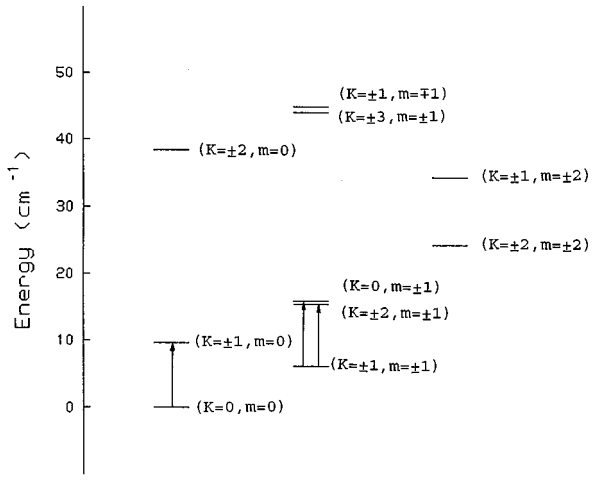

FIG. 1. Energy-level diagram for HSH--NH_3 for the ground vibrational state assuming free internal rotation. The J structure is suppressed. The energy levels were calculated using Eq. (1) with the estimated spectroscopic constants of Herbine *et al.* (Ref. 11). The transitions observed in the present study are shown by the arrows. The $m=0$ levels are of A symmetry and the $m=\pm1$ and $m=\pm2$ levels are of E symmetry. Note that collisional relaxation of the $K=\pm1$, $m=\pm1$ level to the $K=0$, $m=0$ level is nuclear-spin forbidden ($A\leftrightarrow E$ transitions are collisionally and electric-dipole forbidden).

blocks, with the A symmetry block having $m=0,\pm3,\pm6,\cdots$ and the E symmetry block having $m=\pm1,\pm2,\pm4,\pm5,\pm7,\cdots$.

The main features of the energy-level structure of HSH--NH_3 is obtained by evaluating the diagonal matrix elements of H in the $|JKMm\rangle$ basis with $V_3=0$ to give

$$E(J,K,m)=\frac{(B+C)}{2}J(J+1)+\left(A-\frac{B+C}{2}\right)K^2 - 2QKm+Fm^2. \tag{5}$$

Evaluation of $E(J,K,m)$ using $A=291\,201$ MHz, $B=3247$ MHz, $C=3212$ MHz, $F=476\,873$ MHz, and $Q=291\,201$ MHz, as estimated by Herbine *et al.*[11] from the structure of HSH--NH_3, gives the energy-level diagram shown in Fig. 1. Here, we have suppressed the J structure by setting $J=0$ in the expression for $E(J,K,m)$.

As seen in Fig. 1, the lowest energy state for the A symmetry species has $K=0$, $m=0$. For the E symmetry species the states are doubly degenerate, with the lowest energy state having $K=\pm1$, $m=\pm1$, with $Km>0$. The $K=0$, $m=0$, A symmetry state correlates to the $K=0$ state of free NH_3, while the $K=\pm1$, $m=\pm1$, $Km>0$, E symmetry states correlate to the $K=1$ state of free NH_3. Symmetry and nuclear-spin selection rules prevent the A and E species of NH_3 or of the complex from interconverting radiatively or collisionally in the expansion. The consequence of this selection rule is that at the cold molecular-beam temperatures of the expansion most of the population lies in the $K=0$, $m=0$ state and in the metastable $K=\pm1$, $m=\pm1$, $Km>0$ state. Consideration of the b type $\Delta K=\pm1$, $\Delta m=0$ selection rules together with the metastability of the $K=\pm1$, $m=\pm1$, $Km>0$ state indicates that the strongest submillimeter bands will be those shown by arrows in Fig. 1. Note that the frequency for these three bands are all estimated to be near $\nu\approx A\approx291$ GHz, assuming $A\gg B+C$. The μ_b axis component of the dipole moment, which is responsible for the intensity of the $\Delta K=\pm1$ bands is estimated by Herbine *et al.*[11] to be 0.6 D in the free-rotor limit.

HSH proton tunneling

In addition to the internal-rotation motion, the spectrum is complicated by a tunneling motion that interchanges the bonded and nonbonded protons on the H_2S subunit. This large-amplitude motion splits each $|J,K,m\rangle$ state into a symmetric and antisymmetric tunneling component, as shown

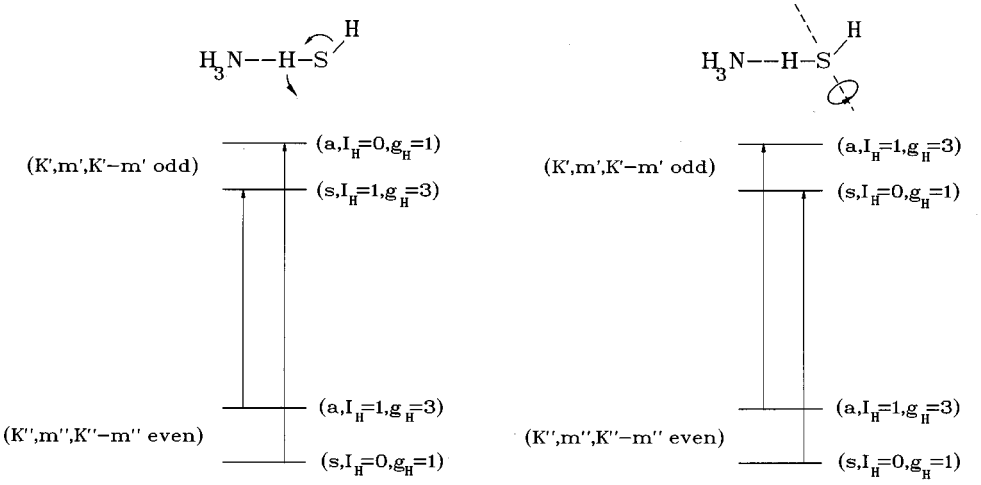

FIG. 2. Energy-level diagrams showing the tunneling state selection rules for the b-type, $\Delta K=\pm1$, $\Delta m=0$, transitions for two possible H_2S proton-interchange tunneling pathways in HSH--NH_3. Each J level of a K,m state is split into a symmetric and antisymmetric tunneling component due to the tunneling interchange of the two H_2S protons. For the tunneling pathway on the left, μ_b is an antisymmetric function of the tunneling coordinate while on the right μ_b is a symmetric function of the tunneling coordinate. The tunneling selection rules on the left are thus $a\leftrightarrow s$ in the tunneling state while on the right they are $a\leftrightarrow a$ and $s\leftrightarrow s$ in the tunneling state. The relative statistical weights of the transitions due to the H_2S proton spin functions is given by $g_I=2I_H+1$, where I_H is the resultant proton nuclear spin of the H_2S protons.

schematically in Fig. 2, where we present energy-level diagrams and selection rules for two possible tunneling pathways for the proton interchange. In the left side of Fig. 2 we have assumed a tunneling pathway in which the *b* dipole moment component of the complex, μ_b, is an antisymmetric function of the tunneling coordinate. Such a tunneling pathway may be pictured as a partial rotation of the H_2S subunit about its *c* inertial axis, which is normal to the plane of the H_2S. In the right side of the figure we have assumed a tunneling pathway in which μ_b is a symmetric function of the tunneling coordinate. In this case the tunneling pathway could be pictured as a partial rotation of the H_2S moiety about its C_2 symmetry axis. As seen in the figure, for μ_b antisymmetric, the $\Delta K=\pm 1$ transitions require a change tunneling state, while for μ_b symmetric, no change in tunneling state occurs. For HOH--NH_3 the observed selection rules are only consistent with the left side of the figure.

Fermi–Dirac statistics dictate that the relative statistical weight factors for the symmetric (s) and antisymmetric (a) tunneling states are in a 3:1 ratio, since the tunneling motion interchanges the two equivalent spin 1/2 protons on the H_2S unit. The relative statistical weights are given by $g_I \equiv 2I_H+1$, where $I_H=1$ or 0 is the resultant proton nuclear spin for the H_2S protons. Total statistical weight factors and symmetry labels for the rovibronic species of the nonrigid HSH--NH_3 complex are most conveniently determined by classifying the wave functions in the molecular symmetry group G_{12}, which is isomorphic to the D_{3h} point group.[18] In G_{12}, the $m=0$, $K=0$, s state has a total proton nuclear-spin statistical weight of 4 while the a state has a total weight of 12 and, similarly, the $m=\pm 1$, $K=\pm 1$, $Km>0$, s state has a weight of 4 and the a state has a weight of 12.

Spectroscopic results

A sample $K=1\leftarrow 0$ spectrum for HSH--NH_3 showing the $Q(1)-Q(11)$ transitions is presented in Fig. 3. The Q-branch lines are assigned to the $m=0$, A state transition of Fig. 1. Two Q branches are observed (upper and lower panels in Fig. 3), with a 3:1 intensity ratio, indicative of a tunneling splitting arising from the interchange of the two protons on the H_2S subunit. The separation between the Q branches is approximately 1729 MHz, with the singlet H_2S proton spin component being higher in frequency. These observations are consistent with the energy-level diagram given in the left side of Fig. 1, indicating that μ_b is an antisymmetric function of the tunneling coordinate. The tunneling splitting is determined to be 864 MHz, which is one half the separation of the two Q branches. To associate the observations with the energy-level diagram on the right side of Fig. 1 would require us to invoke a large difference between the tunneling splittings in the lower and upper states to give an observed splitting of 1729 MHz. We note, however, that the observed singlet–triplet splittings are independent of K and m for the bands studied, making it unlikely that there is any significant K or m dependence to the tunneling splittings. This result, together with the agreement of the frequency ordering predicted from the left side of Fig. 2 with experiment, leads us to conclude that μ_b must be an antisymmetric function of the tunneling coordinate.

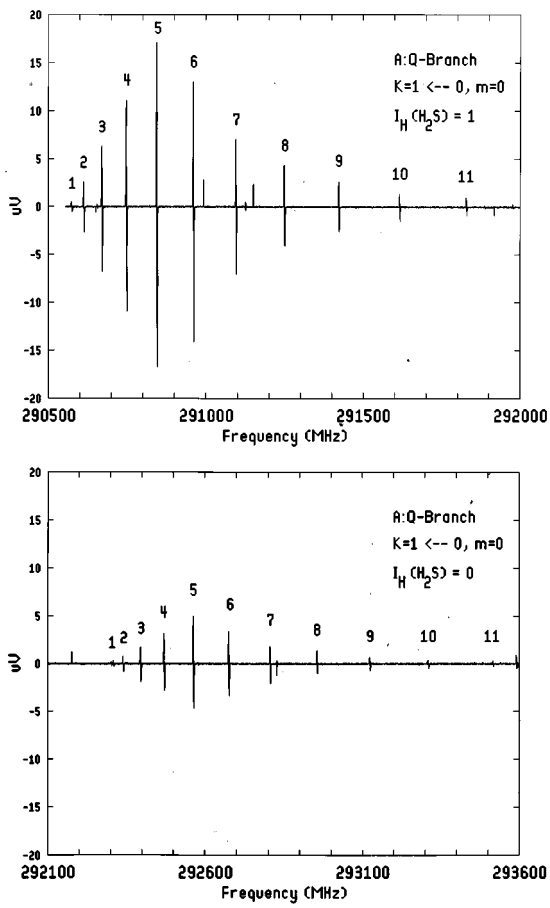

FIG. 3. Sample spectrum showing the $J=1$–11 lines of the *b* type $K=1\leftarrow 0$, $m=0$, A-symmetry Q-branch transitions for HSH--NH_3. Two Q branches are observed with a 3:1 relative intensity ratio. The weaker Q branch (lower panel) arises from the $K=0$ symmetric tunneling state with a resultant H_2S proton spin of $I_H=0$ and relative statistical weight of $g_I=1$, and the stronger Q-branch (upper panel) arises from the $K=0$ antisymmetric tunneling state with $I_H=1$ and $g_I=3$. The spectrum was recorded at a frequency scan rate of approximately 1.5 MHz/s using a time constant of 125 ms. The unusual intensity pattern within a Q branch is a consequence of the quadrupole focusing field which makes the intensities of the lines also dependent on the focusing behavior of the upper and lower states in the electrostatic field.

In addition to the A state spectrum of Fig. 3, transitions were also observed for the E state, $m=\pm 1$, $K=0\leftarrow\pm 1$, and $K=\pm 2\leftarrow\pm 1$ subbands, and the H_3N--$H^{34}SH$ (4.2% natural abundance) A state, $m=0$, $K=1\leftarrow 0$ subband. The observed transitions are given in Table I. We have supplemented the previous a type, $\Delta K=0$ data of Herbine *et al.*[11] with additional microwave and radiofrequency measurements. The radiofrequency measurements were made using radiofrequency-submillimeter double-resonance to probe the asymmetry doublet splitting in the $K=1$, $m=0$, A state. The observation of these transitions verifies the J assignment and establishes that the transitions belong to the A state. For the $|K|>0$, E states the large a-type Coriolis interaction arising from the $-2Q\mathbf{jJ}_a$ splittings lifts the near degeneracy of the asymmetry doublets, giving an ''asymmetry'' doublet splitting of ~ 40 cm^{-1}. For these states the only radiofrequency spectrum is below ~ 4 MHz, and corresponds to direct transitions across the ^{14}N nuclear–quadrupole hyperfine struc-

TABLE I. Observed submillimeter transitions for HSH--NH_3 in MHz.[a]

	$K=1\leftarrow0$, $m=0$, A		$K=\pm2\leftarrow\pm1$, $m=\pm1$, E $Km>0$		$K=0\leftarrow\pm1$, $m=\pm1$, E $Km\geqslant0$		$K=1\leftarrow0$, $m=0$, A, ^{34}S	
	I_H[b]$=1$	$I_H=0$	$I_H=1$	$I_H=0$	$I_H=1$	$I_H=0$	$I_H=1$	$I_H=0$
$P(9)$					236 206.22			
$P(8)$			234 954.24		242 639.73			
$P(7)$			241 415.90		249 084.37	250 785.90		
$P(6)$	251 454.70		247 875.46	249 575.50	255 537.00	257 245.12		
$P(5)$	258 020.92	259 733.26	254 332.58	256 038.76	261 995.68	263 709.19	258 070.78	
$P(4)$	264 567.79	266 286.36	260 789.68	262 500.61	268 458.04	270 176.44	264 492.28	266 203.11
$P(3)$	271 094.93	272 818.60	267 247.64	268 961.88			270 895.01	272 610.33
$P(2)$					281 386.58		277 277.95	
$P(1)$					287 850.14			
$Q(1)$	290 575.08	292 303.56			294 313.96			
$Q(2)$	290 613.67	292 340.91			294 311.32	296 034.82		
$Q(3)$	290 671.47	292 396.67			294 308.51	296 028.47		
$Q(4)$	290 748.65	292 471.41			294 305.70	296 021.85		
$Q(5)$	290 844.87	292 564.76		288 347.06	294 305.70	296 016.43		
$Q(6)$	290 960.81	292 676.62		288 336.48	294 308.51	296 013.48		292 085.53
$Q(7)$	291 095.79	292 807.27		288 322.20	294 317.64			292 211.50
$Q(8)$	291 250.15	292 957.12	286 615.61	288 297.08			290 655.75	292 355.83
$Q(9)$	291 423.81	293 124.63	286 588.84	288 260.23			290 822.77	
$Q(10)$	291 616.59	293 311.91	286 548.76	288 208.60			291 008.92	
$Q(11)$	291 828.49	293 516.85	286 493.30					
$Q(12)$	292 059.86	293 740.99						
$Q(13)$	292 310.44	293 983.50						
$Q(14)$	292 580.49							
$Q(15)$	292 869.15							
$Q(16)$	293 177.19							
$R(0)$							296 308.52	
$R(1)$	303 424.11	305 149.90			307 237.56	308 962.21	302 612.42	
$R(2)$	309 825.13	311 547.32	306 028.63	307 742.76			308 892.55	
$R(3)$			312 492.33				315 152.86	316 862.62
$R(4)$		324 272.71			326 614.98		321 391.42	323 094.59
$R(5)$	328 895.80		325 408.15				327 607.68	329 303.56
$R(6)$							333 801.72	

[a]Experimental uncertainties on line positions are estimated as $1\sigma=0.25$ MHz.
[b]I_H is the resultant proton nuclear spin for the H_2S protons.

ture. A sample A-state double-resonance spectrum is shown in Fig. 4.

The transitions of Tables I and II were least-squares fit to the frequencies calculated from the energy-level expression

$$W(J,K,\mathrm{sym})=\nu_0+\bar{B}J(J+1)-DJ^2(J+1)^2+\delta_{A,\mathrm{sym}}\delta_{|K|,1}(-1)^{J+K_a+K_c}\times\frac{B-C}{4}J(J+1), \quad (6)$$

where $\bar{B}=(B+C)/2$, B, and C are rotational constants, D is a centrifugal distortion constant, and ν_0 is a subband origin. The $B-C$ term is necessary to describe the asymmetry splitting of the $K=1$, A state. The energy-level expression is written using the fact that the A symmetry, $m=0$, $K=0$ and $K=1$ states have an energy-level structure qualitatively similar to that of a rigid asymmetrical top, allowing us to use the limiting prolate and pseudo-oblate quantum numbers, K_a and K_c, to label the transitions.

The spectroscopic constants determined from the least-squares fit of the frequencies are given in Table III. We also tabulate the tunneling splittings, $\nu_t=[\nu_0(I_H=0)-\nu_0(I_H=1)]/2$, for the various subbands studied. All the

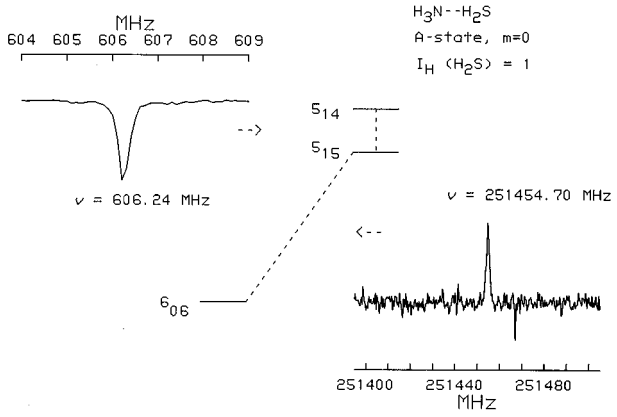

FIG. 4. Sample radiofrequency-microwave double-resonance spectrum of HSH--NH_3. The microwave oscillator was set to the $5_{15}\leftarrow6_{06}$ transition for the $I_H=1$ state of HSH--NH_3 and the radiofrequency oscillator was tuned through the $5_{14}\leftarrow5_{15}$ transition. The strong double-resonance transition is observed because the states involved in the microwave transition are either nonfocused (5_{15}) or weakly focused (6_{06}) by the quadrupole field, whereas the 5_{14} transition on which the radiofrequency transition terminates is strongly focused by the quadrupole field. The double-resonance spectrum corresponds to approximately 20 s of signal averaging time.

TABLE II. Observed *a*-type radiofrequency and microwave transitions for HSH--NH_3 in MHz.[a]

	I_H[b]=1	I_H=0	I_H=1, ^{34}S
A state, $m=0$			
$3_{12}-3_{13}$	242.56		233.90
$4_{13}-4_{14}$	404.22	412.25	389.85
$5_{14}-5_{15}$	606.24		
$1_{01}-0_{00}$	6 466.080[c]	6 466.610[c]	
$2_{02}-1_{01}$	12 931.827[c]	12 932.869[c]	
$5_{05}-4_{04}$	32 323.26	32 325.76	
$6_{06}-5_{05}$	38 783.83	38 786.93	
$3_{13}-2_{12}$	19 333.73		
$4_{14}-3_{13}$	25 776.80	25 773.73	
$5_{15}-4_{14}$	32 218.00	32 212.93	
E state, $K=\pm1$, $m=\pm1$, $Km>0$			
4–3	25 850.15	25 852.18	
5–4	32 309.93	32 312.55	
6–5	38 768.02	38 771.18	

[a]Experimental uncertainties on line positions are estimated as $1\sigma=0.25$ MHz, unless otherwise noted.
[b]I_H is the resultant proton nuclear spin for the H_2S protons.
[c]From Ref. 11. The estimated experimental uncertainties (1σ) are 10 kHz for the $1_{01}-0_{00}$ transitions and 25 kHz for the $2_{02}-1_{01}$ transitions.

transitions are weighted unity in the fit, except for the more precise $J=1\leftarrow0$ and $2\leftarrow1$ measurements of Herbine *et al.*,[11] which are weighted 100. The standard deviations, σ, of the fits range from 0.14–0.43 MHz, close to our estimated experimental precision of 0.25 MHz.

Proton interchange tunneling barrier

Here, we use a one-dimensional model to determine the barrier separating the two isoenergetic minima associated with the H_2S proton interchange tunneling. We will assume, consistent with the observed tunneling-state transition selection rules, that the tunneling motion can be pictured as a partial internal rotation of the H_2S unit about its *c* inertial axis. We will further assume that the H_2S motion is completely uncoupled from the NH_3 unit, allowing us to approximate the reduced mass for tunneling by the *c*-axis moment of inertia of free H_2S, $I_{cc}(H_2S)$. The experimental results are consistent with this latter assumption. For instance, we find that the experimental tunneling splittings vary by less than 1% for the *K* and *m* states studied, indicating that the tunneling is only weakly coupled to the NH_3 internal rotation. In fact, this decoupling of the H_2S tunneling and the NH_3 internal rotation is strong evidence for a small barrier to NH_3 internal rotation. For nonzero internal rotation barriers these two motions are necessarily strongly coupled, since the NH_3 unit must rotate by 60° about its symmetry axis in order for the H_2S tunneling to bring the complex to an isoenergetic configuration.

The tunneling is modeled using the Hamiltonian,

$$H_{\text{tun}}=F\mathbf{p}^2+V(\theta), \tag{7}$$

where $F=\hbar^2/[2I_{cc}(H_2S)]$, $V(\theta)$ is the large amplitude potential, θ is the acute angle between the C_2 axis of H_2S and the assumed linear H_3N--HS bond, and $\mathbf{p}=-i\hbar(d/d\theta)$. The transition state for $V(\theta)$ is at $\theta=0$ and the two equilibrium configurations are at $\theta=\pm\theta_e\equiv\pm46.1°$. We consider two models for the large amplitude potential. The first model approximates $V(\theta)$ by a quartic potential of the form,

$$V(\theta)=V_b\left[\left(\frac{\theta}{\theta_e}\right)^4-2\left(\frac{\theta}{\theta_e}\right)^2\right], \tag{8}$$

where V_b is the height of the tunneling barrier. The Hamiltonian matrix for H_{tun} is set up in a harmonic oscillator basis and diagonalized to determine the tunneling splitting.

TABLE III. Spectroscopic constants for HSH--NH_3 in MHz.[a]

	$K=1\leftarrow0$, $m=0$		$K=1\leftarrow0$, $m=0$, ^{34}S	
	I_H[a]=1	I_H=0	I_H=1	I_H=0
ν_0	293 788.081 (83)	295 516.95 (14)	293 156.93 (21)	294 877.71 (34)
B'	3 232.593 5 (58)	3 232.344 (10)	3 171.387 (35)	3 171.144 (30)
D'	0.014 99(16)	0.014 98(31)	0.014 431(68)	0.013 90(92)
$(B-C)'$	40.422 3 (68)	41.211 (16)	38.978 (23)	39.765 (29)
B''	3233.077 7 (53)	3 233.338 0 (80)	3 171.847 (33)	3 172.087 (28)
D''	0.014 95(16)	0.014 96(30)	0.014 335(67)	0.013 78(88)
σ[b]	0.22	0.31	0.39	0.17
ν_t	864.4		860.4	
	$K=0\leftarrow\pm1$, $m=\pm1$, $Km\geq0$		$K=\pm2\leftarrow\pm1$, $m=\pm1$, $Km>0$	
	I_H=1	I_H=0	I_H=1	I_H=0
ν_0	291 083.22 (15)	292 810.00 (12)	296 330.65 (22)	298 047.87 (38)
B'	3 231.003 (30)	3 230.715 8 (79)	3 232.250 (19)	3 232.020 (43)
D'	0.000 75(48)	0[d]	0.028 53 (27)	0.028 90(87)
B''	3 231.715 (23)	3 231.985 (11)	3 231.707 (22)	3 231.950 (49)
D''	0.014 80(30)	0.014 84(16)	0.014 88 (29)	0.014 64(90)
σ[b]	0.31	0.14	0.32	0.43
ν_t[c]	863.4		858.6	

[a]Experimental uncertainties are one standard error from the least-squares fit.
[b]Standard deviation of the least-squares fit in MHz.
[c]Proton interchange tunneling splitting, $\nu_t=[\nu_0(I_H=0)-\nu_0(I_H=1)]/2$.
[d]Constrained in the least-squares fit.

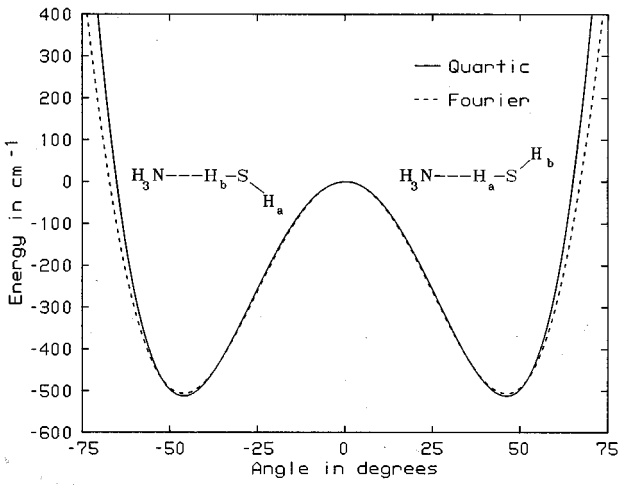

FIG. 5. Plot of two model potentials discussed in the text for the H_2S proton interchange tunneling in HSH--NH_3. The tunneling barrier is determined to be 510(3) cm^{-1}.

For the second approximation to $V(\theta)$ we consider the Fourier model of Stockman *et al.*[6] where the potential is approximated as

$$V(\theta)=\frac{V_1}{2}(1-\cos\theta)+\frac{V_2}{2}(1-\cos 2\theta), \tag{9}$$

with the constraint that $V_1=-4V_2\cos\theta_e$. For this potential the matrix elements of H_{tun} are evaluated in the free-rotor basis set, $|m\rangle=e^{im\theta}(2\pi)^{-1/2}$.

The quartic and Fourier potentials which reproduce the observed experimental 864.4 MHz, $m=0$ tunneling splitting are shown in Fig. 5. As seen in the figure the potentials are strikingly similar. The difference between the 513 cm^{-1} barrier for the quartic potential and the 507 cm^{-1} barrier for the Fourier potential is less than 2%. The Fourier model when applied to HOH--NH_3 requires a 840 cm^{-1} to reproduce the 57 MHz HOH tunneling splitting.[6] Attempts to correct the model for the effect of an inplane geared coupling of the H_2O tunneling with the NH_3 bending gives a barrier of 704 cm^{-1}.[6] Consistent with expectations, the present results show that the N--HS bending potential in HSH--NH_3 is less anisotropic than the N--HO bending potential in HOH--NH_3.

Internal-rotation barrier

The present results are consistent with a near vanishing barrier to internal rotation. In the free-rotor limit, assuming that the NH_3 top axis is coincident with the a inertial axis, the band origins, ν_0, for the three observed $K',m\leftarrow K'',m$ subbands depend only on $A-(B+C)/2$ and Q. Examination of Eq. (5) leads to the following expressions for the origins of the observed bands:

$$\nu_0(K=1,m=0\leftarrow K=0,m=0)=A-\frac{B+C}{2}, \tag{10a}$$

$$\nu_0(K=0,m=\pm1\leftarrow K=\pm1,m=\pm1,Km>0)$$
$$=-\left(A-\frac{B+C}{2}\right)+2Q, \tag{10b}$$

$$\nu_0(K=\pm2,m=\pm2,Km>0\leftarrow K=\pm1,m=\pm1,Km>0)$$
$$=3\left(A-\frac{B+C}{2}\right)-2Q. \tag{10c}$$

Removing the effects of H_2S tunneling by taking the average of the $I_H=1$ and $I_H=0$ band origins in Table III for the ν_0's in Eqs. (10a) and (10b) gives $A-[(B+C)/2]=294.65$ GHz and $Q=293.30$ GHz. Using these values in Eq. (10c) predicts a band origin for the $K=\pm2$, $m=\pm1$, $Km>0\leftarrow K=\pm1$, $m=\pm1$, $Km>0$ transition of 297.36 GHz, surprisingly close to the observed value of 297.19 GHz.

Model calculations with the A, B, C, F, and Q values of Herbine *et al.*[11] and with nonzero internal-rotation barriers, V_3, indicate that Eqs. (10a)–(10c) break down as the barrier is increased. Indeed, we find that the equations poorly describe the calculated band origin positions for V_3 barriers above 10 cm^{-1}. For instance, if we fit the calculated band origins to Eq. (10a) and (10b) to determine effective $A-(B+C)/2$ and Q and use these values in Eq. (10c) to predict the calculated band origin for the $K=\pm2$, $m=\pm1$, $Km>0\leftarrow K=\pm1$, $m=\pm1$, $Km>0$ transition we obtain errors of 0, 0.2, 0.7, 3, and 6 GHz for $V_3=0$, 5, 10, 20, and 30 cm^{-1}, respectively. When we do this same procedure with the experimental frequencies we obtain an error of 0.2 GHz, similar to the $V_3=5$ cm^{-1} model calculation error. Allowing for some model uncertainty leads us to conservatively report the barrier as $V_3=5(3)$ cm^{-1}.

The $V_3=5(3)$ cm^{-1} barrier in HSH--NH_3 can be compared to the 10.5(50) cm^{-1} barrier determined by Stockman *et al.*[6] for the related HOH--NH_3 complex. The slightly larger barrier in the HOH complex may be the result of the shorter distance in this complex between the nonbonded H atoms on the donor and acceptor units compared to the HSH complex. For a linear hydrogen bonded structure the nonbonded H--H distance is 3.60 Å in HOH--NH_3 and 4.08 Å in the HSH--NH_3. The nonbonded H--H distances are significantly larger than the 2.3 Å H--H separation found in ethane where $V_3\sim1024$ cm^{-1}.

CO_2-Laser photodissociation

Photodissociation via excitation of the NH_3 umbrella mode of the HSH--NH_3 complex is observed on the $R(48)$ (991.6 cm^{-1}), $R(50)$ (992.5 cm^{-1}), and $R(52)$ (993.4 cm^{-1}) lines of the 10 μm band of the $^{12}CO_2$ laser. The observed photodissociation places an upper bound on the zero-point dissociation energy of the complex. The center of the feature (992.5 cm^{-1}) is blueshifted by ~43 cm^{-1} from the hypothetical inversion-free NH_3 monomer umbrella vibration at 949.9 cm^{-1}. Unlike HSH--NH_3, the HOH--NH_3 complex is not dissociated by a single CO_2-laser (10 μm) photon. The umbrella mode of HOH--NH_3 is observed near 1021 cm^{-1}, blueshifted ~71 cm^{-1} from the NH_3 monomer mode. In Table IV we list band origins[12,19,20] for several NH_3 complexes. The magnitude of the blueshift of the vibration from that of the monomer correlates with the binding energy of the complex; the complexes with the largest blueshifts (NCH--NH_3 and HOH--NH_3) are not dissociated by excitation of the NH_3 umbrella mode.

TABLE IV. Band origins and frequency shifts (in cm^{-1}) for the NH_3 umbrella vibrations in several weakly bound complexes.[a]

Complex	ν_0	$\Delta\nu$
H_3N--N_2O[b]	980	30
H_3N--OCS[b]	982	32
H_3N--HCCH[b]	984	35
H_3N--CO_2[b]	987	37
H_3N--HSH[c]	993	43
H_3N--HOH[d]	1021	71
H_3N--HCN[e]	1042	92

[a]Experimental uncertainties are 2 cm^{-1} or less.
[b]Reference 19.
[c]Present work.
[d]Reference 12.
[e]Reference 20.
[f]Frequency shift form the inversion free monomer vibration at 949.9 cm^{-1}.

CONCLUSION

The present results furnish the first detailed information on the large amplitude motions in the HSH--NH_3 complex. The barrier has been determined to be 510(3) cm^{-1} for the HSH proton interchange tunneling and 5(3) cm^{-1} for the NH_3 internal rotation. Consistent with the low barrier to internal rotation, no evidence has been found for any significant coupling of the two large amplitude motions despite the fact that the two motions are necessarily strongly interacting in the high barrier limit. Finally, we have placed an upper bound on the zero-point bond dissociation energy of the complex of 992.5 cm^{-1} from observation of photodissociation upon excitation of the NH_3 umbrella mode at 992.5 cm^{-1}. The large amplitude-barriers and CO_2-laser results are all consistent with a significantly stronger hydrogen-bonding interaction in HSH- -NH_3 than in HOH- -NH_3. The present results when combined with the similar results on the HOH--NH_3 complex offer two well characterized and related systems for the test of simple potential models.

ACKNOWLEDGMENTS

We would like to thank NATO (Grant No. 921-278), the Russian Fund for Fundamental Studies, and the Internal Science Foundation (Registration No. Ph3-1137) for partial support of this work.

[1] For a recent review see, K. L. Leopold, G. T. Fraser, S. E. Novick, W. Klemperer, Chem. Rev. **94** 1807 (1994).
[2] T. R. Dyke, B. J. Howard, and W. Klemperer, J. Chem. Phys. **56**, 2442 (1972).
[3] N. Ohashi and A. S. Pine, J. Chem. Phys. **81**, 73 (1984).
[4] R. E. Bumgarner, S. Suzuki, P. A. Stockman, P. G. Green, and G. A. Blake, Chem. Phys. Lett. **176**, 123 (1991).
[5] R. E. Bumgarner, J. Bowen, and G. A. Blake, Forty-Fifth Symposium on Molecular Spectroscopy, Columbus, OH, June 16–20 (1990).
[6] P. A. Stockman, R. E. Bumgarner, S. Suzuki, and G. A. Blake, J. Chem. Phys. **96**, 2496 (1992).
[7] G. T. Fraser, R. D. Suenram, L. H. Coudert, R. S. Frye, J. Mol. Spectrosc. **137**, 244 (1989).
[8] G. T. Fraser, R. D. Suenram, L. H. Coudert, J. Chem. Phys. **90**, 6077 (1989).
[9] G. T. Fraser, A. S. Pine, R. D. Suenram, J. Chem. Phys. **91**, 637 (1989).
[10] Yu. I. Alekshin, G. M. Altshuller, O. P. Pavlovsky, E. N. Karyakin, A. F. Krupnov, D. G. Paveliev, and A. P. Shkaev, Int. J. Infrared Millimeter Waves **11**, 961 (1990).
[11] P. Herbine, T. A. Hu, G. Johnson, and T. R. Dyke, J. Chem. Phys. **93**, 5485 (1990).
[12] G. T. Fraser and R. D. Suenram, J. Chem. Phys. **96**, 7287 (1992).
[13] T. E. Gough, R. E. Miller, and G. Scoles, Appl. Phys. Lett. **30**, 338 (1977).
[14] T. R. Dyke, in *Structure and Dynamics of Weakly Bound Molecular Complexes*, edited by A. Weber (Reidel, Boston, 1987).
[15] P. Herbine and T. R. Dyke, J. Chem. Phys. **83**, 3768 (1985).
[16] R. W. Kilb, C. C. Lin, and E. B. Wilson, Jr., J. Chem. Phys. **26**, 1695 (1957).
[17] J. D. Swalen and D. R. Hershbach, J. Chem. Phys. **27**, 100 (1957).
[18] P. R. Bunker, *Molecular Symmetry and Spectroscopy* (Academic, New York, 1979).
[19] G. T. Fraser, D. D. Nelson, Jr., A. Charo, and W. Klemperer, J. Chem. Phys. **82**, 2535 (1985).
[20] G. T. Fraser, A. S. Pine, W. A. Kreiner, and R. D. Suenram, Chem. Phys. **156**, 523 (1991).